NJC

Accepted Manuscript

This is an *Accepted Manuscript*, which has been through the Royal Society of Chemistry peer review process and has been accepted for publication.

Accepted Manuscripts are published online shortly after acceptance, before technical editing, formatting and proof reading. Using this free service, authors can make their results available to the community, in citable form, before we publish the edited article. We will replace this *Accepted Manuscript* with the edited and formatted *Advance Article* as soon as it is available.

You can find more information about *Accepted Manuscripts* in the Information for Authors.

Please note that technical editing may introduce minor changes to the text and/or graphics, which may alter content. The journal's standard Terms & Conditions and the Ethical guidelines still apply. In no event shall the Royal Society of Chemistry be held responsible for any errors or omissions in this *Accepted Manuscript* or any consequences arising from the use of any information it contains.

ROYAL SOCIETY OF CHEMISTRY

www.rsc.org/njc

Journal Name

ARTICLE

Template-directed Approach to Two-dimensional Molybdenum Phosphide-Carbon Nanocomposites with High Catalytic Activities in Hydrogen Evolution Reaction

Received 00th January 20xx,
Accepted 00th January 20xx

DOI: 10.1039/x0xx00000x

www.rsc.org/

Zhaoquan Yao,[a] Yuezeng Su,*[,a] Chenbao Lu,[a] Chongqing Yang,[b] Zhixiao Xu,[b] Jinhui Zhu,[b] Xiaodong Zhuang*[,b] and Fan Zhang*[,b]

Abstract: At first, we developed a new two-dimensional graphene-based Schiff base porous polymer (TPP) by the condensation of melamin, 1,4-phthalaldehyde and aminated graphene oxide. Then, we prepared a new family of two-dimensional (2D) molybdenum phosphide-containing porous carbons (TPC-MoPs) by using the as-prepared TPP as 2D template, and low-cost diammonium phosphate and ammonium molybdate as precursors through stepwise self-assembly and pyrolysis performances. The resulting TPC-MoPs feature layered and porous structures with the high specific surface areas up to 72 $m^2 g^{-1}$. The unique mophorlogy characters render such kinds of materials with the inceased active catalytic sites and better conductivity as compared with the other MoPs-based composites. As a consequence, the as-prepared composites exhibit superior electrocatalytic performance in the hydrogen evolution reaction (HER) under acidic conditions, with a Tafel slope of 68.5 mV dec^{-1}, a low onset overpotential of 65 mV (versus the reversible hydrogen electrode), and a large exchange current density (j_0) of 0.144 mA cm^{-2}.

1. Introduction

Fossil fuels currently provide most of the world's energy, but are continuously diminishing.[1] As an alternative, hydrogen represents one of most promising clean and renewable energy.[2, 3] Direct electrocatalytic water splitting has become one of the simplest, cleanest, and most-efficient ways to produce hydrogen gas on a large scale.[4] However, this process requires the use of efficient electrocatalysts for the activation of the H–O bond in water in the hydrogen evolution reaction (HER) at a low working voltage.[5] Although some noble metal catalysts, such as Pt and Pd, exhibit superior electrocatalytic performance for the HER, their scarcity and high price hinder commercial applications.[6] A large number of low cost electrocatalysts have been explored, mainly including (1) metal-free heteroatom-doped carbon-based materials (e.g., carbon nanotubes[7, 8], graphene[9, 10], and carbon nitride[11, 12]) and (2) non-noble transition metal carbides, oxides, sulfides or phosphide (e.g., molybdenum[13-16], iron[17, 18], cobalt[19-21], copper[22, 23], tungsten[24-26] and nickel[27, 28]) , and (3) the composites comprising transition-metal nanoparticles and porous carbons.[29]

Recently, transition metal phosphides (TMPs) have exhibited great potential as high-performance catalysts for HER,[30-32] but still far from the practical applications due to their insufficient activity, durability and complicated preparation procedure. In order to overcome these drawbacks, some efforts have been done mainly in two directions: (1) increasing the number of the exposed active sites; (2) improving the conductivity.[29] For example, nanoscale (~4 nm) and amorphous molybdenum phosphide (MoP) nanoparticles[30] or MoP nanoparticles with interconnected networks[33] as high-performance HER catalysts, have been developed by exposing a greater number of active sites in these materials. Titanium foil MoP[34] and nickel-foam-supported NiSe[35] have been prepared by using the electrically conductive substrates. However, to our best knowledge, it is still rarely reported to form a composite with improved catalytic activities by tailoring the morphology. Graphene possessing high electrical conductivity,[36] a large theoretical specific surface area,[37] and excellent thermal/chemical stability[38] has been considered as a two-dimensional (2D) template for the preparation of various nanocomposites . In this aspect, we have developed graphene template-directed approach to form 2D graphene-based porous polymers or porous carbons, and exploring their application in a wide scope of energy conversion and storage materials, such as supercapacitor[39] and oxygen reduction reaction electrocatalysts.[40] On the other hand, very recently, we reported molybdenum phosphide-containing porous carbon as highly active catalysts for electrochemical water splitting.[29] On the basis of above consideration and our previous work, we are trying to develop a new strategy assess to TMP-based composites with high catalytic activities in HER through constructing 2D nanostructures.

Herein, we present the large-scale preparation of MoP-containing 2D porous carbons (TPC-MoPs) through a simple protocol by uniformly dispersing $(NH_4)_6Mo_7O_{24}$ and $(NH_4)_2HPO_4$

[a] School of Aeronautics and Astronautics, and School of Electronic Information and Electrical Engineering, Shanghai Jiao Tong University, 800 Dongchuan RD, Shanghai 200240, P.R. China, E-mail: yzsu@sjtu.edu.cn.
[b] School of Chemistry and Chemical Engineering, State Key Laboratory of Metal Matrix Composites, Shanghai Jiao Tong University, 800 Dongchuan RD, Shanghai 200240, P. R. China, E-mail: zhuang@sjtu.edu.cn, fan-zhang@sjtu.edu.cn.

in the pore canal and surface of a 2D graphene-based Schiff base porous polymer (TPP), and then pyrolysis treatment, in which TPP were readily prepared by the condensation of aminated graphene oxide, melamine and 1,4-phthalaldehyde. The as-prepared TPC-MoPs exhibited outstanding electrochemical catalytic activities for HER (in 0.5 M H_2SO_4), with an overpotential of up to 126 mV at 10 mA cm^{-2} and an exchange current density of 1.44×10^{-4} A cm^{-2}.

2. Experimental

Organic solvents were dried and distilled under nitrogen atmosphere. The flake graphite was purchased from Aldrich. All other chemicals were purchased from Aladdin, Aldrich and Adamas, and used without further purification.

2.1 Materials preparation:

Preparation of aminated graphene oxide (AGO). Graphene oxide (GO) was synthesized from flake graphite according to a modified Hummer's method. Freeze dried GO (1.0 g) was added to anhydrous DMF (300 mL) and ultrasonicated for 24 h. Then, *N*-hydroxysuccinimide (NHS, 3.4 g) and *N*-(3-(dimethylamino) propyl)-*N*'-ethylcarbodiimide hydrochloride (EDC·HCl, 5.7 g) were added to the GO dispersion at 0 ℃. After stirring for a few hours, 1,3-diaminopropane (2 mL) was added, and the mixture was stirred for another 10 h at room temperature. Then washing with DI water and ethanol, after repeating the operation for several times and followed by vacuum drying at 40℃ overnight, aminated graphene oxide (AGO) was produced.

Synthesis of two-dimensional Schiff-base porous polymer (TPP). Dry AGO (1 equiv, *weight*) was dispersed in anhydrous dimethyl sulfoxide (DMSO) with the aid of ultrasonication. Then, melamine and *p*-phthalaldehyde (6 equiv, molar ratio is 2:3) were added to the dispersion. After nitrogen bubbling for 2 hours, the mixture was heated to 180 ℃ for 72 h under nitrogen atmosphere. Before cooling to room temperature, the precipitate was isolated by quick filtration and then washed with excess DMF and acetone. After Soxhlet fraction for 3 days using THF as solvent and vacuum drying at room temperature, sandwich-type two-dimensional Schiff-base porous polymer (TPP) was offered as fluffy powders in a yield of 80% .

Preparation of two-dimensional (2D) molybdenum phosphide-containing porous carbons (TPC-MoP). TPP (1.0 g) was added to the aqueous solution of $(NH_4)_6Mo_7O_{24}{\cdot}4H_2O$ (0.75 g, 0.6 mmol) and $(NH_4)_2HPO_4$ (561 mg, 4.2 mmol). After vigorously stirred at 90 ℃ for 10 h, the precipitate was filtrated and vacuum dried at 120 ℃. The dry sample which denoted as salt@TPP was then pyrolyzed at 850 ℃ for 4 h in hydrogen/argon (5wt%/ 95wt%). As-produced molybdenum phosphide embedded two-dimensional porous carbon was denoted as TPC-MoP-1. In the control experiment, TPC-MoP-2, TPC-MoP-3, TPC-MoP-4 were prepared via the same method by using 0.5, 1 and 1.5 equivalent of $(NH_4)_6Mo_7O_{24}{\cdot}4H_2O$ and $(NH_4)_2HPO_4$ without changing the amount of TPP. Molybdenum phosphide (MoP) was prepared by pyrolysis of the mixture of $(NH_4)_6Mo_7O_{24}{\cdot}4H_2O$ and $(NH_4)_6HPO_4$ (molar ratio for Mo:P = 1:1) at 850℃ for 4 h in hydrogen/argon (5wt%/ 95wt%). The physically mixed TPC and MoP was also prepared as the control sample and denoted as TPC/MoP.

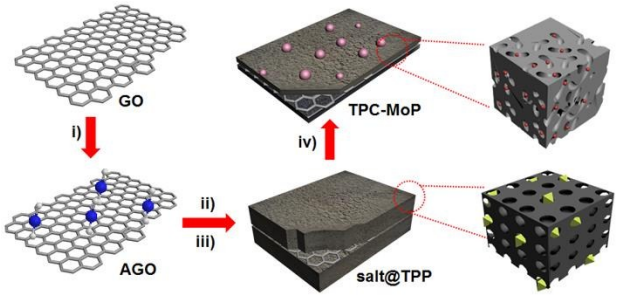

Scheme 1. Preparation of TPC-MoPs. (i) Dimethylformamide, 1,3-diaminopropane, N-hydroxysuccinimide, EDC·HCl, room temperature; (ii) melamine, terephthalaldehyde, anhydrous dimethyl sulfoxide, 180°C, argon, 3 days; (iii) $(NH_4)_6Mo_7O_{24}{\cdot}4H_2O$, $(NH_4)_2HPO_4$, 90°C overnight, then dried at 120°C; (iv) hydrogen/argon (5%/95%), 850°C, 4 h. GO, graphene oxide; AGO, aminated GO; polyhedrons and spheres represent the salts and MoP particles embedded in the pores, respectively.

Preparation of two-dimensional porous carbon (TPC). As-prepared TPP was used as precursor to prepare nitrogen-doped two-dimensional porous carbon (TPC) by direct pyrolysis at 850℃ for 4 h in hydrogen/argon (5wt%/ 95wt%).

2.2 Instruments

X-ray diffraction (XRD) measurements were conducted through Bruker D8 Advance X-ray diffractometers with Cu Kα radiation (k-1.54 Å) at a generator voltage of 40 kV and a generator current of 50 mA with a scanning speed of 6° min^{-1} from 5° to 80°. Fourier transform infrared spectroscopy was performed on a Spectrum 100 (Perkin Elmer, Inc., USA) spectrometer with a scan range of 4000-400 cm^{-1}. The samples were pulverized with KBr and pressed into disks. The Inductively Coupled Plasma (ICP) was performed using iCAP6300 ICP-AES (Thermo Scientific, USA). Scanning electron microscopy (SEM) was conducted through an FEI Sirion-200 (FEI Co., USA) field emission scanning electron microscope. Transmission electron microscopy (TEM) observations were performed with a JEOL-2100 (JEOL Ltd., Japan) electron microscopy at an operating voltage of 200 kV. The nitrogen sorption and desorption isotherms were measured through the Autosorb-iQA3200-4 analyzer (Quantatech Co., USA). X-ray photoelectron spectroscopy (XPS) experiments were conducted through on an AXIS Ultra DLD system (Kratos) with Al Kα radiation as X-ray source for radiation.

2.3 Electrochemical Measurements

The electrochemical measurements were carried out using a CHI660D potentiostat (CH Instruments, China) in a typical three-electrode setup in 0.5 M H_2SO_4 solution, a glass carbon electrode (Dia 5.61 mm) as the working electrode, a Pt wire as the counter electrode, and an Ag/AgCl (4 M KCl) electrode as the reference electrode. In the experiment of 4000 cyclic voltammetry (CV) sweeps (sweep rate: 100 mV s^{-1}), the Pt wire was replaced by a graphite rod as the counter electrode. In all measurements, the Ag/AgCl (4 M KCl) reference electrode was calibrated with respect to reversible hydrogen electrode (RHE). A flow of N_2 was maintained over the electrolyte during the experiment to eliminate dissolved oxygen. Linear sweep

voltammetry (LSV) was conducted in 0.5 M H_2SO_4 with a sweep rate of 5 mV s^{-1}, and all the LSV curves were iR-corrected by using the CHI software. In this present study, we choose the start voltage of Tafel regions as the onset overpotentials.[41] Electrochemical impedance spectroscopy (EIS) were conducted in the same configuration at η=125 mV from 10^6 – 0.02 Hz with an AC voltage of 5 mV. To calculate the C_{dl} values, CV curves were measured with different scan rate, from 10 mV s^{-1} to 125 mV s^{-1}, and C_{dl} = 0.5×Slope, $\Delta j = j_a - j_c$. All the potentials reported in our manuscript are against RHE, E (RHE) = E (Ag/AgCl) + 0.214 V, in 0.5 M H_2SO_4.[29]

Glass carbon electrode (Pine Instrument Company) was polished with a 0.05 μm and 0.3 μm alumina slurry on a microcloth, and then rinsed with ultrapure water and ethanol. After a while, the electrode was treated with sonication in ultrapure water for 15 min, then dried under a gentle nitrogen atmosphere after being washed with ultrapure water. For the working electrode preparation, 5 mg as-prepared catalysts were dispersed in 500 μL solvent (a mixture of Nafion (5wt%, 50 μL) and ethanol (450 μL)) under sonication for 30 minutes to form a homogeneous ink. And then 6 μL of catalyst suspension was slightly loaded on the pre-polished electrode, as well as a catalysts loading of 0.243 mg cm^{-2}. For comparison, 20% Pt/C, a commercially available catalyst, was loaded on the electrode in the same way (0.024 mg cm^{-2}). The electrodes were then dried at room temperature before measurement.

3. Results and discussion

3.1 Morphology and structure characterization

The preparation of TCP-MoPs was presented in **Scheme 1**. Firstly, 2D graphene-based porous polymer (TPP) was synthesized by the condensation of aminated graphene oxide as template, with melamine and *p*-phthalaldehyde as building blocks. Then, the TPP was used as 2D template to uniformly adsorb transition metal and phosphorous-containing ions (e.g., $Mo_7O_{24}^{6-}$ and HPO_4^{2-}) via self-assembly processing. The resulting salt-loaded TPP (salt@TPP) were further pyrolysized at 850°C for 4 h under a reducing atmosphere (H_2/Ar, 5%/95%), to afford the TPC-MoP samples. The concise preparation protocol on the basis of the low-cost starting materials makes it possible to achieve the targeted composites (TPP-MoP-n) (n = 1, 2, 3, 4 with respect to the different MoP weight contents) in a large scale (~1.0 kg).

In order to further understand the structures of the as-prepared TPC-MoPs, X-ray diffraction (XRD) analyses were performed. As shown in **Figure 1a** and Figure S1, the characteristic peaks for TPC-MoP-*n* (*n* = 1, 2, 3, 4) were observed at 27.9°, 32.3°, 27.9°, 43.1°, 57.4°, 57.9°, 64.9°, and 74.3°, corresponding to the (001), (100), (101), (110), (002), (111), (200), (102), and (201) faces of MoP, respectively. All of these diffraction peaks for TPC-MoPs are agreed well with the standard pattern of MoP (JCPDS#65-6487) and the MoP control sample, revealing the high crystalline character of the MoP comonent in these TPC-MoP-n samples.

Scanning electron microscopy (SEM) and transmission electron microscopy (TEM) were used to reveal the morphology

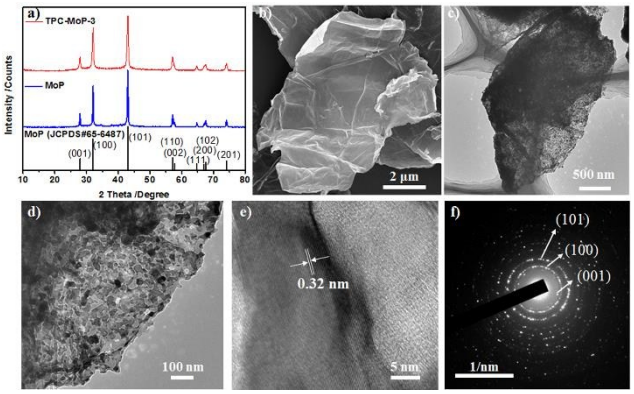

Figure 1. (a) XRD patterns of MoP and TPC-MoPs. (b) SEM image of TPC-MoP-3. (c, d) TEM images of TPC-MoP-3. (e) HR-TEM image of embedded MoP particles; (f) SAED pattern of TPC-MoP-3.

and microstructure of TPC-MoPs. As an example, the sample TPC-MoP-3 was systematically investigated. The SEM image of TPC-MoP-3 (Figure 1b) clearly shows a large number of nanosheets, demonstrating a maintained 2D morphology arising from TPP template even under the deposition of $(NH_4)_6Mo_7O_{24}$ and $(NH_4)_2HPO_4$ and pyrolysis treatment. The TEM images (Figure 1c and 1d) indicate a large amount of nanoparticles with a size ranging from 30 to 50 nm uniformly dispersed on the2D graphene-based porous carbon sheets (TPC). The TEM images of the other samples for TPC-MoP-n (n = 1, 2, 4) also show similar 2D morphologies and MoP particle microstructures (Figures S2, S3, and S4). The high-resolution TEM (HR-TEM) image (Figure 1e) exhibits a typical 001 plane of MoP with an interplanar spacing of 0.32 nm, which is in accordance with the peak at 28° in the XRD pattern. The selected-area electron diffraction (SAED) (Figure 1f) indicated that the crystal structure of of TPC-MoP-3 is quite similar to that of the bare MoP salt (Figure S5). Furthermore, the uniform distribution of MoP in the 2D porous carbon for TPC-MoP-3 was

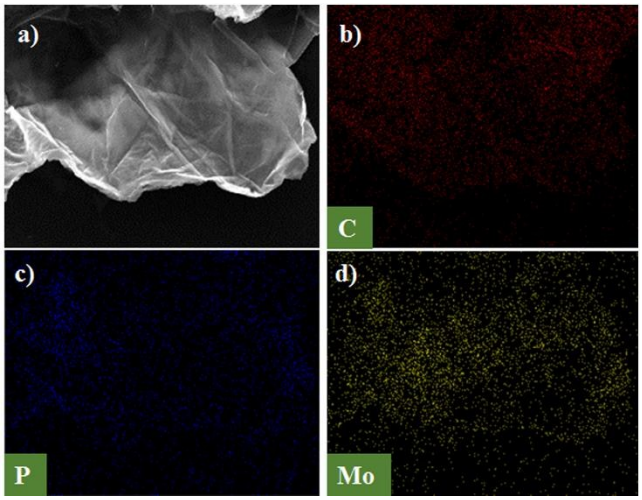

Figure 2. SEM-EDX images of (a) stacked TPC-MoP-3 nanosheets, (b) carbon, (c) phosphorous, and (d) molybdenum elemental mapping of the stacked TPC-MoP-3 nanosheets.

observed by SEM with energy-dispersive X-ray spectroscopy (SEM-EDX) over a large region (Figure 2).

X-ray photoelectron spectroscopy (XPS) was carried out to elucidate the valence states of the individual elements of TPC-MoPs. The survey (Mo 3d, P 2p, and N 1s spectra for MoP, the TPC, and TPC-MoP-3) was illustrated in **Figure 3**. In the survey spectrum of TPC-MoP-3 (Figure 3a), the C, Mo, and P signals were obvious. In the Mo 3d XPS profile, the peaks at a binding energy of 231.44 eV/228.30 eV (Mo3, $3d_{3/2}/3d_{5/2}$) can be ascribed to MoP, which matches the previous reports well.[34] The peaks at 236.48 eV/233.26 eV (Mo1, $3d_{3/2}/3d_{5/2}$) and 235.23 eV/232.10 eV (Mo2, $3d_{3/2}/3d_{5/2}$) can be assigned to the oxidized Mo species of MoP[32] on the surface of the sample and the high oxidation state of Mo of MoO_3,[31] respectively, with no efficient electrocatalytic activity.[42, 43] This result is consistent with reported similar systems[31] due to residual oxidation of MoP occurs only on the surface (less than 10 nm). The Mo 3d spectra of TPC-MoP-1, TPC-MoP-2, and TPC-MoP-4 show similar results (Figure S6). The P 2p XPS spectrum of TPC-MoP-3 (Figure 3c) exhibits two doublets at binding energies of 134.31 eV/133.47 eV and 130.41 eV/129.53 eV, which can be attributed to surface oxides and MoP,[31] respectively. Both the TPC and TPC-MoP-3 exhibited similar N 1s spectra mainly at a binding energy of 401.2 eV, corresponding to quaternary N (N2).[40] Due to partly overlapping with Mo 3p3/2 of MoP, the N 1s signals at 402.7 eV (N1: pyridine-*N*-oxide) and 398.3 eV (N3: pyridinic N) for TPC-MoP-3 are not well resolved. These results revealed that MoP component has been efficiently incoroperated into the N-doped porous carbon nanosheets.

Inductively coupled plasma (ICP) analysis was used to confirm the component contents in the as-prepared TPC-MoPs (Table S1). The Mo and P contents by weight in TPC-MoP-*n* (*n* = 1, 2, 3, 4) are 45.8%,14.6%; 52.3%, 16.3%; 55.5%, 16.8% and 68.7%, 20.7%, respectively. Remarkably, almost the same molar ratios of Mo/P (1.04 ± 0.03) were observed in these TPC-MoP-*n* samples. TPC-MoP-4 has the highest MoP loading percentage of 89.4%.

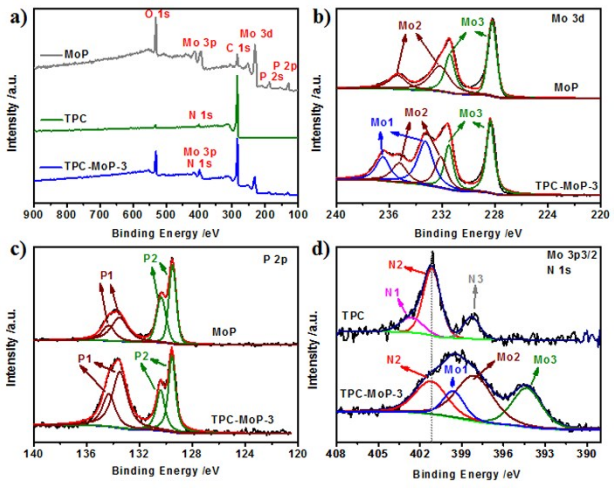

Figure 3. XPS analysis of the as-synthesized TPC, MoP, and TPC-MoP-3. (a) XPS survey spectra of MoP, the TPC, and TPC-MoP-3. (b) Mo 3d XPS spectra of MoP and TPC-MoP-3. (c) P 2p XPS spectra of MoP and TPC-MoP-3. (d) N 1s XPS spectra of the TPC and TPC-MoP-3 (partly overlapped with Mo 3p3/2 of MoP).

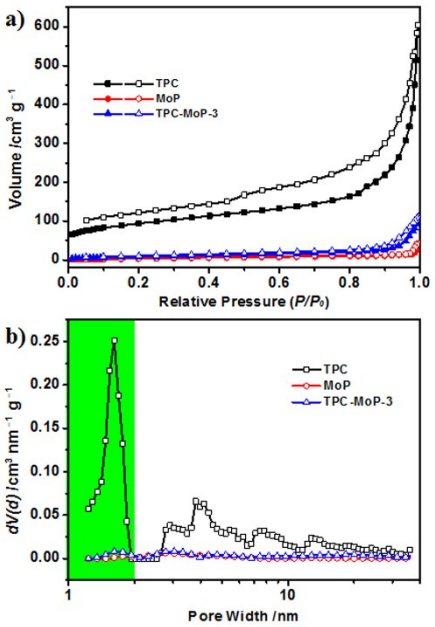

Figure 4. (a) Nitrogen sorption (solid symbols)/desorption (open symbols) isotherms and (b) pore size distributions of the TPC, MoP, and TPC-MoP-3.

Table 1. Nitrogen physisorption properties of the as-prepared materials.

Sample	S_{BET} [a] [$m^2\ g^{-1}$]	S_{Lang} [b] [$m^2\ g^{-1}$]	D_{av} [c] [nm]	V_{tot} [d] [$cm^3\ g^{-1}$]
TPP	371	471	11.7	1.085
TPC	336	426	11.1	0.934
MoP	18	41	14.8	0.066
TPC-MoP-1	72	135	15.4	0.276
TPC-MoP-2	49	113	13.1	0.162
TPC-MoP-3	31	53	22.1	0.171
TPC-MoP-4	26	65	11.5	0.075

Surface area calculated from the nitrogen adsorption isotherms based on the [a]BET and [b]Langmuir models; [c]average pore size; [d]total pore volume calculated at P/P_0 = 0.99.

The porous nature of TPC-MoPs, MoP, and the TPC were investigated by nitrogen sorption/desorption analyses at 77 K. It was found that the isotherms of all the materials exhibited type II nitrogen sorption according to the IUPAC classification (**Figure 4a** and Figure S7a).[44] The specific surface areas for TPC-MoP-3, MoP, and the TPC were 31, 18, and 336 $m^2\ g^{-1}$, respectively, on the basis of Brunauer–Emmett–Teller (BET) calculations (**Table 1**). The average pore size calculated by AsiQwin software (Quantatech Co., USA) for TPC-MoP-3, MoP, and the TPC were 22.1, 14.8, and 11.1 nm, respectively. The differences between TPC and TPC-MoP-3 in the surface areas and pore structures were likely ascribed that the continuous porous framework of TPC, might be occupied by the MoP particles in TPC-MoP-3. Similarly, the specific surface areas are delinced from TPC-MoP-1 to TPC-MoP-4) as the increase in the

equivalent Mo/P precursors due to the partial pore filling and increase in mass. The rich porous structures not only offer a uniformly distributed channel for adsorbing molybdenum/phosphorous precursors but they also avoid aggregation during the production of MoP nanoparticles under high temperature. These structures enable the facile access of the ions into the framework as a result of capillary diffusion, which is likely beneficial to the uniform incorporation of the metal phosphide throughout the 2D porous carbon scaffold.

3.2 Electrocatalytic HER Activity

Given that MoP has been widely known as one of the best electrochemical catalysts for the HER, the catalytic performance in the HER for the as-prepared TPC-MoP-n was carried out in 0.5 M H_2SO_4 solution at a scan rate of 5 mV s^{-1}, using a typical three-electrode set-up at room temperature, by depositing the catalysts with the same loading of 0.243 mg cm^{-2} on a glassy carbon electrode (GCE) (as described in the experimentalsection). The polarization curves of MoP and TPC-MoP-*n* were shown in **Figure 5a**. Considering the effect of ohmic resistance on the intrinsic behavior of the catalysts, iR-corrected curves were used for rational comparison. It was found that TPC-MoP-3 exhibited the lowest onset overpotential (65 mV) in comparison with the TPC-MoP-1 (112 mV), TPC-MoP-2 (83 mV), TPC-MoP-4 (78 mV), and MoP (120 mV), as seen in Figure 5a. A further negative potential sweep led to a sharp rise in the current density, which reached 10 and 100 mA cm^{-2} at overpotentials of 126 and 239 mV for TPC-MoP-3, respectively. This result suggests that MoP nanoparticles dispersed in the 2D porous carbon is likely beneficial to HER performance than the bare MoP. TPC-MoP-3 shows the best HER performence among TPC-MoP-n.

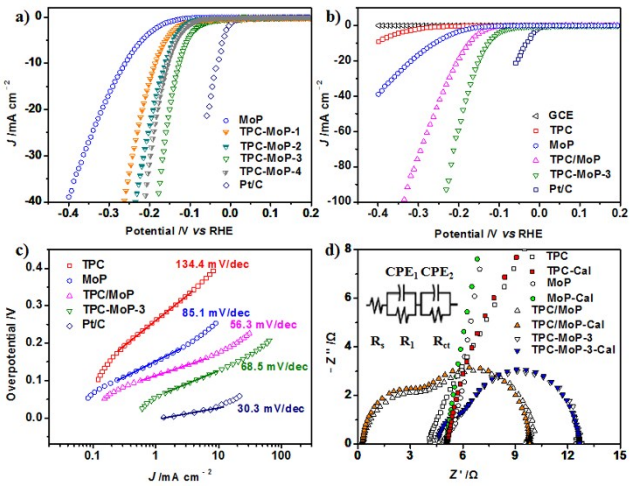

Figure 5. Electrochemical-catalyzed HER performance of the as-prepared materials in 0.5 M H_2SO_4. (a) Polarization curves for the MoP, TPC-MoP-1, TPC-MoP-2, TPC-MoP-3, TPC-MoP-4, and Pt/C with a scan rate of 5 mV s^{-1}. (b) Polarization curves for the GCE, TPC, MoP, TPC/MoP, TPC-MoP-3, and Pt/C with a scan rate of 5 mV s^{-1}. (c) Tafel plots for the TPC, MoP, TPC/MoP, TPC-MoP-3, and Pt/C. (d) Nyquist plots and fitting plots of TPC, MoP, TPC/MoP, TPC-MoP-3 recorded at η=125 mV (versus the RHE) (inset: equivalent circuit).

Table 2. HER performance of the as-prepared materials (η_{10} at 10 mA cm^{-2}, η_{100} at 100 mA cm^{-2}).

Sample	Tafel slope [mV dec^{-1}]	Tafel region [mV]	J_0 [mA cm^{-2}]	η_{10} [mV]	η_{100} [mV]
TPC	134.4	191–340	1.15×10^{-5}	>400	—
MoP	85.1	120–190	1.68×10^{-5}	260	>400
TPC/MoP	56.3	100–160	9.76×10^{-6}	174	338
TPC-MoP-1	83.5	112–185	6.12×10^{-5}	185	362
TPC-MoP-2	60.1	83–150	2.36×10^{-5}	160	343
TPC-MoP-3	68.5	65–130	1.44×10^{-4}	126	239
TPC-MoP-4	61.7	78–120	3.78×10^{-5}	154	>400
Pt/C	30.3	0–20	1.81×10^{-3}	32	—

The Tafel plots for MoP, TPC-MoP-*n*, and Pt/C were shown in Figure S8. The linear portions of the Tafel plots were fitted to the Tafel equation $\eta = b \log(j) + a$, where η is the overpotential, b is the Tafel slope, j is the current density, and a is the Tafel intercept relative to the exchange current density j_0. Therefore, the Tafel slopes for MoP, TPC-MoP-1, TPC-MoP-2, TPC-MoP-3, TPC-MoP-4, and Pt/C can be easily calculated as 85.1, 83.5, 60.1, 68.5, 61.7, and 30.3 mV dec^{-1}, respectively. The Tafel slopes for TPC-MoP-*n* (n = 1, 2, 3, 4) did not reach the Tafel slopes of 29, 38, and 116 mV dec^{-1} correlated with a different rate-determining step of the HER,[45] revealing that the HER catalyzed by TPC-MoP-*n* proceeds via a Volmer–Heyrovsky mechanism.[46] The exchange current density (j_0) of TPC-MoP-3 was 0.144 mA cm^{-2}, nearly three times that of TPC-MoP-1, and much larger than of MoP, TPC-MoP-2, and TPC-MoP-4 (**Table 2**).

In order to further understand the role of the porous carbon matrix of TPC-MoPs in the improvement of HER performance, as comparison, we measured the HER performance of a sample consisting of the mixture of TPC and MoP (denoted as TPC/MoP) with the same weight content of MoP as that of TPC-MoP-3. In Figure 5b and 5c, TPC/MoP exhibited current densities of 10 and 100 mA cm^{-2} at overpotentials of 174 and 338 mV, respectively, and the Tafel slope was 56.3 mV dec^{-1}, which are better than those of neat MoP. Such results were probably ascribed to the improved electrical conductivity with the addition of TPC. In order to confirm this, electrochemical impedance spectroscopy was employed to study the conductivities of the as-prepared materials. Nyquist plots and fitting plots of the TPC, MoP, TPC/MoP, and TPC-MoP-3 were shown in Figure 5d and Figure S9. In the inset equivalent circuit of Figure 5d, R_{ct} is the charge-transfer resistance, which is inversely proportional to the rate of electron transfer; CPE is the constant phase element; and R_s is the solution-phase resistance; R1 electrode porosity resistance. The calculated results based on the equivalent circuit were listed in Table S2. As proposed, TPC/MoP (6.0Ω) and TPC-MoP-3 (6.7Ω) exhibited a much lower charge-transfer resistance than the neat MoP sample (186.1Ω). TPC-MoP-3 was found to be a superior catalyst to TPC/MoP prepared by physical mixing, which could be attributed to the intrinsic

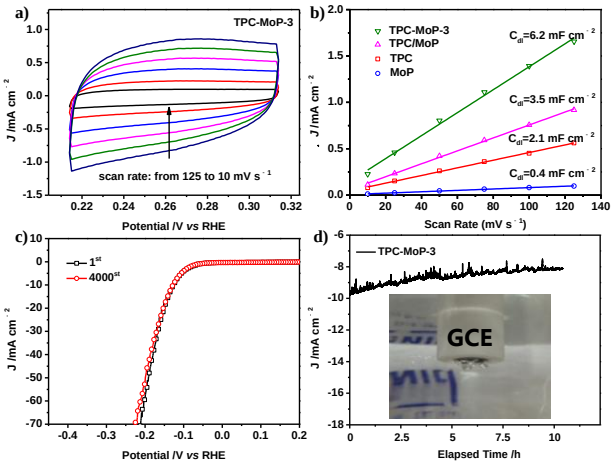

Figure 6. (a) CV curves for TPC-MoP-3 at different rates from 10 to 125 mV s^{-1}. (b) Capacitive current at 0.264 V versus the RHE (0.05 V versus Ag/AgCl) as a function of the scan rate for TPC-MoP-3, TPC/MoP, MoP, and the TPC ($\triangle j = ja - jc$). (c) Polarization data for TPC-MoP-3 in 0.5 M H_2SO_4 initially and after 4000 CV sweeps between +0.1 and –0.4 V versus RHE. (d) Chronoamperometric electrolysis in 0.5 M H_2SO_4 at η = 125 mV versus the RHE.

structural characters of the former one, such as porous structure and MoP nanoparticles, formed by its template-directed preparation method.

A larger effective active surface area means more catalytically active sites,[47] but the effective surface area cannot be measured directly. Using a simple cyclic voltammetry (CV) method, we determined the double-layer capacitance (C_{dl}), which is expected to be linearly proportional to the effective active surface area.[48] As show in **Figure 6a** and Figure S10, CV curves for the TPC, MoP, TPC/MoP, and TPC-MoP-*n* in the region of 0.214–0.314 V versus the RHE were carried out at 10, 25, 50, 75, 100, and 125 mV s^{-1}. The C_{dl} for TPC-MoP-3 was calculated as 6.2 mF cm^{-2}, which is much larger than that for the TPC (0.4 mF cm^{-2}), MoP (2.1 mF cm^{-2}), and TPC/MoP (3.5 mF cm^{-2}). These results strongly suggest that TPC-MoP-3 has a larger effective active surface area for the HER. Moreover, the CV sweeps between +0.2 V and –0.4 V (versus the RHE) at a scan rate of 100 mV s^{-1} were carried out to evaluate the stability of TPC-MoP-3. As shown in Figure 6c, after 4000 CV sweeps, the polarization curve exhibited the negligible loss of the cathodic current density in comparison with the initial polarization curve. Chronoamperometric electrolysis provided evidence of the remarkable stability of TPC-MoP in 0.5 M H_2SO_4 at an applied overpotential of 125 mV (versus the RHE) (Figure 6d), and just a little current degradation was observed after electrolysis for more than 10 h. This result suggests the good stability of TPC-MoP-3 even after a long-term electrochemical process.

In general ,the outstanding electrocatalytic activity in HER for TPC-MoP-3 can be ascribed to the following: (1) MoP-nanoparticles uniformly dispersed in the whole porous carbon matrix, give rise of much more catalytic active sites ; (2) 2D porous carbon matrix not only serves as a strong supportor for stablizing and well dispersing the MoP particles against aggregation, but also provides a long-distance conductive medium favorable for charge transfer.

4. Conclusions

Upon stepwise self-assembly and pyrolysis performances, a new type of two-dimensional molybdenum phosphide-carbon composites (TPC-MoPs) were successfully achieved by using a 2D graphene-based schiff base porous polymer as a template and commmercial available diammonium phosphate and ammonium molybdate as precursors, offering the unique nanosheets with MoP nanoparticles uniformly dispersed in the porous carbon matrix. The resulting composites exhibited high performance of electrochemical catalysis in HER, as compared with the bare MoP or the other MoP composites, such as MoP prapared on Ti plate,[34] bare MoP,[49] MoP nanoparticles,[31] closed connected MoP,[33] and MoP nanosheets on carbon flake,[50] likely attributable to the increased active catalytic sites and high conductivity, associated with their unique two-dimentional structures. The presented concise synthetic strategy of the nanocomposites can be used to form versatile 2D metal-carbon composites by the combination of various active transition metal salts and graphene-based polymers applicable for the energy-related reactions in a much broader scope, such as the oxygen evolution reaction, the oxygen reduction reaction.

Acknowledgements

The authors thank the financial support from 973 Programs of China (2013CBA01602, 2012CB933400), Natural Science Foundation of China (51403126, 21320102006, 21304057, 21574080) and the Shanghai Committee of Science and Technology (15JC1490500). We also thank the Instrumental Analysis Center of Shanghai Jiao Tong University.

References

1 M. S. Dresselhaus and I. L. Thomas, *Nature*, 2001, **414**, 332.
2 R. M. Dell, D. A. J. Rand, *Hydrogen Energy: Challenges and Prospects*, The Royal Society of Chemistry, Cambridge, UK, 2008, ch. 1.
3 J. A. Turner, *Science*, 2004, **305**, 972.
4 C. Wan, Y. N. Regmi and B. M. Leonard, *Angew. Chem., Int. Ed.*, 2014, **53**, 6407.
5 L. G. Bloor, P. I. Molina, M. D. Symes and L. Cronin, *J. Am. Chem. Soc.*, 2014, **136**, 3304.
6 Jiang, P.; Liu, Q.; Liang, Y.; Tian, J.; Asiri, A. M.; Sun, X. *Angew. Chem., Int. Ed.* 2014, **53**, 12855..
7 W. Cui, Q. Liu, N. Cheng, A. M. Asiri and X. Sun, *Chem. Commun.*, 2014, **50**, 9340-9342.
8 R. K. Das, Y. Wang, S. V. Vasilyeva, E. Donoghue, I. Pucher, G. Kamenov, H. Cheng and A. G. Rinzler, *ACS Nano*, 2014, **8**, 8447.
9 Y. Ito, W. Cong, T. Fujita, Z. Tang and M. Chen, *Angew. Chem., Int. Ed.*, 2014, **54**, 2131.
10 Y. Zheng, Y. Jiao, L. Li, T. Xing, Y. Chen, M. Jaroniec and S. Qiao, *ACS Nano*, 2014, **8**, 5290.
11 M. Shalom, S. Gimenez, F. Schipper, I. H. Cardona, J. Bisquert and M. Antonietti, *Angew. Chem., Int. Ed.*, 2014, **53**, 3654.
12 Y. Zheng, Y. Jiao, Y. Zhu, L. Li, Y. Han, Y. Chen, A. Du, M. Jaroniec and S. Qiao, *Nat. Commun.*, 2014, **5**, 3783.

13 H. Wu, B. Xia, L. Yu, X. Yu and X. Lou, *Nat. Commun.*, 2015, **6**, 6512.
14 L. Wu, X. Wang, Y. Sun, Y. Liu and J. Li, *Nanoscale*, 2015, **7**, 7040.
15 Y. Li, H. Wang, L. Xie, Y. Liang, G. Hong and H. Dai, *J. Am. Chem. Soc.*, 2011, **133**, 7296.
16 Y. Jiao, Y. Zheng, M. Jaroniec and S. Z. Qiao, *Chem. Soc. Rev.*, 2015, **44**, 2060.
17 Z. Zhang, B. Lu, J. Hao, W. Yang and J. Tang, *Chem. Commun.*, 2014, **50**, 11554.
18 D. Wang, M. Gong, H. Chou, C. Pan, H. Chen, Y. Wu, M. Lin, M. Guan, J. Yang, C. Chen, Y. Wang, B. Hwang, C. Chen and H. Dai, *J. Am. Chem. Soc.*, 2015, **137**, 1587.
19 H. Jin, J. Wang, D. Su, Z. Wei, Z. Pang and Y. Wang, *J. Am. Chem. Soc.*, 2015, **137**, 2688.
20 J. Tian, Q. Liu, A. M. Asiri and X. Sun, *J. Am. Chem. Soc.*, 2014, **136**, 7587.
21 Y. Zheng, M. Gao, Z. Yu, Q. Gao, H. Gao and S. Yu, *Chem. Sci.*, 2015, **6**, 4594.
22 P. D. Tran, M. Nguyen, S. S. Pramana, A. Bhattacharjee, S. Y. Chiam, J. Fize, M. J. Field, V. Artero, L. H. Wong, J. Loo and J. Barber, *Energy Environ. Sci.*, 2012, **5**, 8912.
23 J. Tian, Q. Liu, N. Cheng, A. M. Asiri and X. Sun, *Angew. Chem., Int. Ed.*, 2014, **53**, 9577.
24 A. Prabakaran, F. Dillon, J. Melbourne, L. Jones, R. J. Nicholls, P. Holdway, J. Britton, A. A. Koos, A. Crossley, P. D. Nellist and N. Grobert, *Chem. Commun.*, 2014, **50**, 12360.
25 H. Fei, Y. Yang, X. Fan, G. Wang, G. Ruan and J. M. Tour, *J. Mater. Chem. A*, 2015, **3**, 5798.
26 J. Duan, S. Chen, B. A. Chambers, G. G. Andersson and S. Qiao, *Adv. Mater.*, 2015, **27**, 4234.
27 L. A. Stern, L. Feng, F. Song and X. Hu, *Energy Environ. Sci.*, 2015, **8**, 2347.
28 H. Liang, L. Li, F. Meng, L. Dang, J. Zhuo, A. Forticaux, Z. Wang and S. Jin, *Chem. Mater.*, 2015, **27**, 5702.
29 S. Han, Y. Feng, F. Zhang, C. Yang, Z. Yao, W. Zhao, F. Qiu, L. Yang, Y. Yao, X. Zhuang and X. Feng, *Adv. Funct. Mater.*, 2015, **25**, 3899.
30 J. M. McEnaney, J. C. Crompton, J. F. Callejas, E. J. Popczun, A. J. Biacchi, N. S. Lewis and R. E. Schaak, *Chem. Mater.*, 2014, **26**, 4826.
31 P. Xiao, M. A. Sk, L. Thia, X. Ge, R. J. Lim, J. Wang, K. H. Lim and X. Wang, *Energy Environ. Sci.*, 2014, **7**, 2624.
32 T. Wang, K. Du, W. Liu, Z. Zhu, Y. Shao and M. Li, *J. Mater. Chem. A*, 2015, **3**, 4368.
33 Z. Xing, Q. Liu, A. M. Asiri and X. Sun, *Adv. Mater.*, 2014, **26**, 5702.
34 J. Kibsgaard; T. F. Jaramillo, *Angew. Chem., Int. Ed.* 2014, **53**, 14433.
35 C. Tang, N. Cheng, Z. Pu, W. Xing and X. Sun, *Angew. Chem., Int. Ed.*, 2015, **54**, 9351.
36 Y. Ito, W. Cong, T. Fujita, Z. Tang and M. Chen, *Angew. Chem., Int. Ed.*, 2015, **54**, 2131.
37 D. H. Youn, S. Han, J. Y. Kim, H. Park, S. H. Choi and J. S. Lee, *ACS Nano*, 2014, **8**, 5164.
38 C. K. Chua and M. Pumera, *Chem. Soc. Rev.*, 2013, **42**, 3222.
39 X. Zhuang, F. Zhang, D. Wu, N. Forler, H. Liang, M. Wagner, D. Gehrig, M. R. Hansen, F. Laquai and X. Feng, *Angew. Chem., Int. Ed.*, 2013, **52**, 9668.
40 C. Cao, X. Zhuang, Y. Su, Y. Zhang, F. Zhang, D. Wu and X. Feng, *Polym. Chem.*, 2014, **5**, 2057.
41 H. Yan, C. Tian, L. Wang, A. Wu, M. Meng, L. Zhao and H. Fu, *Angew. Chem., Int. Ed.*, 2015, **127**, 6423.
42 H. Vrubel and X. Hu, *Angew. Chem., Int. Ed.*, 2012, **51**, 12703.
43 X. Xie, L. Lin, R. Liu, Y. Jiang, Q. Zhu and A. Xu, *J. Mater. Chem. A*, 2015, **3**, 8055.
44 S. Lowell, J. E. Shields, M. A. Thomas and M. Thommes, *Characterization of Porous Solids and Powders: Surface Area, Pore Size and Density*, Springer, Dordrecht, Netherlands, 2004.
45 C. G. Morales-Guio, L. A. Stern and X. Hu, *Chem. Soc. Rev.*, 2014, **43**, 6555.
46 Y. Zheng, Y. Jiao, M. Jaroniec and S. Z. Qiao, *Angew. Chem., Int. Ed.*, 2015, **54**, 52.
47 C. G. M. Guio and X. Hu, *Acc. Chem. Res.*, 2014, **47**, 2671.
48 M. A. Lukowski, A. S. Daniel, F. Meng, A. Forticaux, L. Li and S. Jin, *J. Am. Chem. Soc.*, 2013, **135**, 10274.
49 X. Chen, D. Wang, Z. Wang, P. Zhou, Z. Wu and F. Jiang, *Chem. Commun.*, 2014, **50**, 11683.
50 W. Cui, Q. Liu, Z. Xing, A. M. Asiri, K. A. Alamry and X. Sun, *Appl. Catal. B: Environ.*, 2015, **164**, 144.

Table of Contents

Template-directed Approach to Two-dimensional Molybdenum Phosphide-Carbon Nanocomposites with High Catalytic Activities in Hydrogen Evolution Reaction

Zhaoquan Yao,[a] Yuezeng Su,*,[a] Chenbao Lu,[a] Chongqing Yang,[b] Zhixiao Xu,[b] Jinhui Zhu,[b] Xiaodong Zhuang,*,[b] Fan Zhang,*,[b]

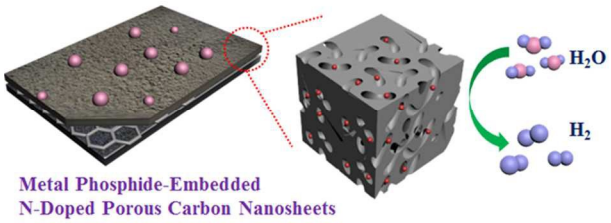

MoP-embedded 2D N-doped porous carbon nanosheets, with excellent electrical conductivity and abundant active sites, performed high catalytic activity in HER.